A Needlescopic Wrist Mechanism With Articulated Motion and Kinematic Tractability for Micro Laparoscopic Surgery

Jongwoo Kim, *Member, IEEE*, Woosub Lee, Sungchul Kang, *Member, IEEE*, Kyu-Jin Cho, *Member, IEEE*, and Chunwoo Kim, *Member, IEEE*

***Abstract*—Invasiveness of laparoscopic surgery can be further reduced by using needlescopic instruments which diameter approaches that of a hypodermic needle. However, such needlescopic instruments are limited by the lack of wrist mechanisms with precise and sharp articulating motion. In this article, we present a two-degree-of-freedom wrist mechanism with articulating motion and enhanced kinematic tractability for micro laparoscopic surgery. The mechanism consists of two highly curved nitinol tubes serially connected by rotary joints whose axes intersect at a remote center of motion (RCM). Its elasticity is only utilized for introducing through a trocar. Once introduced, the rigid body motions of each tube by the rotary joints generate pivoting motion of the attached end-effector about the RCM point. This allows large reorientation of the end-effector's direction with minimal displacement. The serial link structure of the mechanism leads to analytic solutions for tractable kinematics. The design, manufacturing, and the validation of the kinematics of the mechanism are presented, and the feasibility of the mechanism is demonstrated through the peg transfer test using a teleoperated robot system.**

***Index Terms*—Medical applications, medical devices, medical device manufacturing, medical robotics, robot kinematics.**

Manuscript received August 30, 2018; revised March 17, 2019 and August 21, 2019; accepted September 30, 2019. Date of publication October 14, 2019; date of current version February 13, 2020. Recommended by Technical Editor K. Oldham. This work was supported in part by the Korea Institute of Science and Technology Institutional Program under Grant 2E28230 and in part by the National Research Foundation of Korea Grant funded by the Korean Government (MSIP) under Grant NRF-2016R1A5A1938472. *(Corresponding authors: Kyu-Jin Cho and Chunwoo Kim.)*

J. Kim and K.-J. Cho are with the Biorobotics Laboratory/Soft Robotics Research Center/Institute of Advanced Machines and Design, Department of Mechanical and Aerospace Engineering, Seoul National University, Seoul 08826, South Korea (e-mail: kimjongwoo1988@gmail.com; kjcho@snu.ac.kr).

W. Lee and C. Kim are with the Center for Medical Robotics, Korea Institute of Science and Technology, Seoul 02792, South Korea (e-mail: robot@kist.re.kr; cwkim@kist.re.kr).

S. Kang is with the Robot Center, Samsung Research, Seoul 06765, South Korea (e-mail: kasch804@gmail.com).

This article has supplementary downloadable material available at http://ieeexplore.ieee.org, provided by the authors.

Color versions of one or more of the figures in this article are available online at http://ieeexplore.ieee.org.

Digital Object Identifier 10.1109/TMECH.2019.2947072

I. Introduction

LAPAROSCOPIC surgery provides significantly reduced invasiveness compared to the traditional open surgery by replacing a large incision with three to four small incisions for instrument ports. Size of the incision depends on the size of the laparoscopic instruments delivered through the ports, which typically ranges from 5–10 mm in diameter. If the diameter of the instruments is below 3 mm, the invasiveness of the instrument port approaches that of a hypodermic needle and leaves almost no scar. Such a "needlescopic" instruments have been used in various laparoscopic surgeries [1]–[3].

One of the limitations of these needlescopic instruments is the lack of a wrist mechanism for dexterous manipulation of its end-effector. Many surgical instruments equipped with dexterous wrist-like mechanisms have been developed for various applications, ranging from retinal surgery [4], colonoscopy [5], gynecological procedures [6], laparoscopic surgery [7]–[9], arrhythmia [10], atrial fibrillation [11], and skull base surgery [12]. As for the laparoscopic instruments, several instruments with robotic or manual wrist mechanism are commercially available: EndoWrist (Intuitive Surgical, CA, USA) [13], Tuebingen Radius T Surgical System (Tuebingen Scientific Medical GmbH, Tuebingen, Germany) [14], FlexDex (FlexDex, Inc, MI, USA) [15], Covidence SILS (Medtronic, MN, USA) [16]. However, in the size scale of the needlescopic instruments (diameter <5 mm), only a few wrist mechanisms have been developed at the research [17] and commercial level [18].

The biggest challenge in developing a wrist mechanism for the needlescopic instrument is the development of a scalable mechanism. The mechanism has to be scalable in terms of stiffness, manufacturing, and assembly. For example, a tendon-pulley mechanism that has been widely used for the wrist of laparoscopic instruments is not easy to scale down because the length of its moment arm becomes too short to provide enough force and assembly become challenging.

As a result, due to the size constraints, many wrist mechanisms for a needlescopic surgical instruments take the form of continuum robots that generates motion through the deformations of the elastic elements [19]–[21]. In such a "bending wrist" based on the continuum robots, the actuation is embedded in its structure, reducing the complexity. Nevertheless, bending wrist presents limitations in kinematics and motion envelop

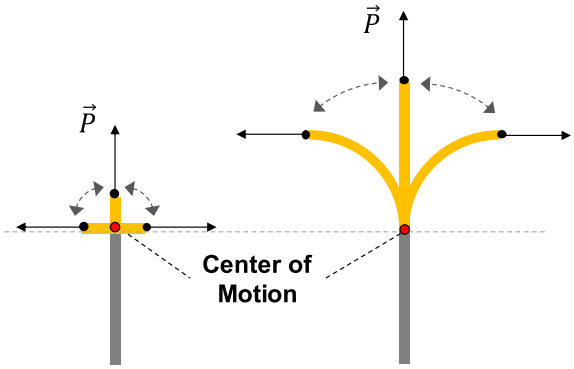

Fig. 1. Comparison of the end-effector motion between articulating wrists (left) and bending wrists (right). The black arrow indicate the unit vector of the tip direction at given configuration. The articulating wrists have sharper turn and better kinematic tractability, and smaller motion envelope compared to the bending wrists.

of the attached end-effector. The solution of the kinematics is complex and often imprecise as it requires solving differential equations and as it is difficult to precisely know the material properties value used in the equations. In addition, due to the length of a bending element and its finite curvature, the end-effector attached to the wrist cannot "pivot" about a point. As a result, reorientation of the end-effector is coupled with large displacement as shown in Fig. 1, increasing its the motion envelope. On the other hand, "articulating wrist" can orient the attached end-effector by rigid body rotation about a fixed point, minimizing the displacement as shown in Fig. 1. Its kinematics is more tractable as it has an analytic solution.

In this article, we present a two degree of freedom (DoF) wrist mechanism that has the remote center of motion (RCM) for microlaparoscopic surgical instruments. The wrist mechanism consists of two links serially connected by revolute joints whose axes intersect at the RCM point. RCM point serves as a fixed pivot point for the articulating motion.

Each link of the proposed wrist consists of a highly precurved nitinol tube fabricated by a special process using asymmetric laser patterning and sequential heat treatment. The mechanism can be scale down to 1.24 mm or less in diameter and fit into a 2 mm trocar for the minimally invasive introduction into the abdominal cavity. Once inside the body, the mechanism can manipulate the orientation of the end-effector only by the combination of the proximal and distal tubes' rotations.

The two main characteristics of the proposed mechanism are the kinematic tractability and the articulated motion at RCM point. The mechanism does not utilize the bending of compliant parts. It solely uses the rotation of two revolute joints. The serial link structure of the mechanism leads to an analytic solution for both forward and inverse kinematics, making it easier and more precise to control. The RCM point of the mechanism serves as a pivot point of a wrist about which the end-effector can change its orientation while maintaining its position. This RCM allows a large reorientation of the end-effector's direction with minimal displacement of the end-effector.

The proposed mechanism is morphologically similar to well-known concentric tube robot [22], [23] in the aspect that both consists of overlapping nitinol tubes. However, concentric tube robots are continuum robot that uses elastic deformation of the precurved nitinol tubes for the actuation. On the other hand, the proposed mechanism is a serial robot in which the tubes are used as serial links actuated by the rotary joints and the motion is generated by rigid body motion of each link. The elasticity of the nitinol tube is only utilized for introducing the mechanism through a trocar.

The contributions of this article include the design of the mechanism considering the range of the articulating motion and kinematic tractability, fabrication method of the high curvature tubes comprising the mechanism, validation of the forward and inverse kinematics model, and demonstration of the mechanism in a teleoperated surgical robot system.

II. Design of the Wrist Mechanism

Compared to other wrist mechanism based on the bending of compliant parts, the proposed mechanism is a serial manipulator with an articulated wrist. As illustrated in Fig. 1, the articulated wrist generates sharp turn of an end-effector that is directly connected to the wrist without bending section. Key design requirement of the mechanism was the range of the articulating motion. The following section describes the kinematic analysis of the mechanism to derive the relationship between the geometry of the link and the range of the articulating motion. From the result of the analysis, the design of the links that generate the articulating motion range of 120°is derived.

A. Overall Structure of the Wrist Mechanism

The wrist mechanism consists of two curved tubes (proximal and distal) that are serially connected by a rotary joint as shown in Fig. 2(a). The first rotary joint is located at the base of the proximal tube and the second joint is located at the base of the distal tube that overlaps with the distal end of the proximal tube. The distal tube is rotated by a three-layered torque coil [24] that are inserted through the proximal tube. The torque coil is capable of transmitting the torque from its proximal to a distal end at a ratio close to 1:1 through the curved path. The torque coil has a sufficiently low flexural rigidity and does not affect the curvature of the structure. The rotations of two tubes generate two-DoFs motion of the tool attached at the end of the tube assembly.

The shape of each curved tube is designed such that the rotation axes of the joints intersect at the point on the distal end of the tube assembly, as shown in Fig. 2(a). Then, this intersection becomes the RCM point whose position remains stationary when the tubes rotate. Therefore, the rotations of the tubes will generate two-DoFs pivoting motion of the tool about the RCM point. The mechanism becomes a wrist that can articulate the attached tools about the RCM point. The complementary multimedia of this article demonstrates the articulating motion of the tool generated by the rotations of the tubes.

B. Design Analysis for the Motion of the Wrist Mechanism

The design parameters that determine the shape of each link in the mechanism are the location $\vec{x}_1$, $\vec{x}_2$ and direction $\vec{\omega}_1$, $\vec{\omega}_2$

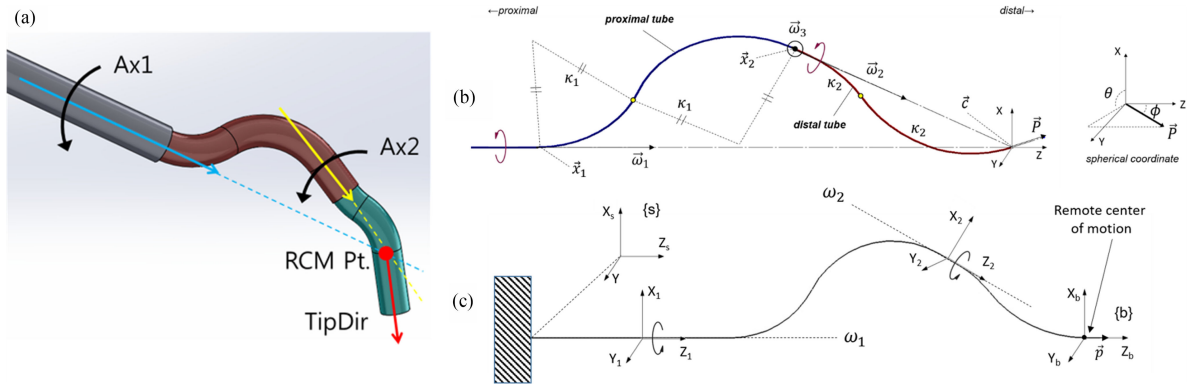

Fig. 2. (a) Structure of the proposed wrist mechanism. (b) Kinematics of each link and tool tip of the wrist mechanism with the direction of the distal tip at the RCM point in the spherical coordinate. The blue line represents the proximal link and the red line represents the distal link, respectively. (c) Coordinates of the wrist mechanism at each link and distal tip to solve the kinematics.

of two rotary joints and the initial direction of the tool $\vec{P}_0$, as shown in Fig. 2(b). RCM point $\vec{c}$ is located at the intersection of the line $\vec{l}_1$ through the point $\vec{x}_1$ parallel to $\vec{\omega}_1$ and line $\vec{l}_2$ through the point $\vec{x}_2$ parallel to $\vec{\omega}_2$. The proximal tube will be a smooth curve interpolating the point $\vec{x}_1$ and $\vec{x}_2$ with the direction of the tangents being $\vec{\omega}_1$ and $\vec{\omega}_2$, respectively. Likewise, the distal tube will be a smooth curve interpolating the point $\vec{x}_2$ and $\vec{c}$ with the direction of the tangents being $\vec{\omega}_2$ and $\vec{P}_0$, respectively. The interpolating curve will have an inflection point, marked by the yellow dot in Fig. 2(b), where the curvature changes its sign. The exact shape of each tube depends on the interpolation method. In this article, each tube was interpolated using two arcs with the same radius but the opposite sign of curvature. κ_1 is the curvature of the proximal tube, κ_2 is the curvature of the distal tube arc.

The relationship between the shape of the curved tubes and the range of the articulating motion about the RCM point was studied. Without loss of generality, we set $\vec{x}_1$ to be the origin $\vec{\omega}_1$ to be the Z-axis. The tool tip initially oriented along $\vec{P}_0$ changes its direction to $\vec{P}$ by rotating the distal tube by θ_2 and then rotating the proximal tube by θ_1

$$\vec{P} = e^{\hat{\omega}_1\theta_1} e^{\hat{\omega}_2\theta_2} \vec{P}_0 \tag{1}$$

where $e^{\hat{\omega}\theta}$ is a rotation matrix given by Rodrigues formula [25] that represents rotation about unit vector axis $\vec{\omega}$ by angle θ.

The range of the articulating motion about the RCM point can be measured by the range of polar angle ϕ and azimuthal angle θ of the tip direction $\vec{P}$. Therefore, $\vec{P}$ is parameterized in spherical coordinate as in (2) where $0 \le \phi \le \pi$, and $0 \le \theta < 2\pi$ in Fig. 2(b)

$$\vec{P} = [\sin\phi\cos\theta, \sin\phi\sin\theta, \cos\phi]^T. \tag{2}$$

For analysis, we define $\vec{\omega}_3 = \frac{(\vec{\omega}_1 \times \vec{\omega}_2)}{|\vec{\omega}_1 \times \vec{\omega}_2|}$, a mutual normal to $\vec{\omega}_1$ and $\vec{\omega}_2$. Since a unit vector can be rotated to any arbitrary direction by combined rotation about two perpendicular axes, $\vec{P}_0$ can be defined by rotating $\vec{\omega}_2$ about $\vec{\omega}_3$ by β, and then rotating about $\vec{\omega}_2$ by α as

$$\vec{P}_0 = e^{\hat{\omega}_2\alpha} e^{\hat{\omega}_3\beta} \vec{\omega}_2. \tag{3}$$

Combining (1) to (3) we have

$$\vec{P} = \begin{bmatrix} \sin\phi\cos\theta \\ \sin\phi\sin\theta \\ \cos\phi \end{bmatrix} = e^{\hat{\omega}_1\theta_1} e^{\hat{\omega}_2\theta_2} e^{\hat{\omega}_2\alpha} e^{\hat{\omega}_3\beta} \vec{\omega}_2. \tag{4}$$

Since $\vec{\omega}_1$ is aligned with the Z-axis, $\vec{\omega}_1 = (0,0,1)^T$, full range of the azimuthal angle, $\theta \in [0, 2\pi)$, can be reached by θ_1. To determine the range of the polar angle ϕ, $\vec{\omega}_1^T$ is multiplied to both sides of (4)

$$\vec{\omega}_1^T e^{\hat{\omega}_1\theta_1} e^{\hat{\omega}_2\theta_2} e^{\hat{\omega}_2\alpha} e^{\hat{\omega}_3\beta} \vec{\omega}_2 = \cos\phi \tag{5}$$

$$\vec{\omega}_1^T e^{\hat{\omega}_2(\theta_2+\alpha)} e^{\hat{\omega}_3\beta} \vec{\omega}_2 = \cos\phi \tag{6}$$

$$\vec{\omega}_1^T e^{\hat{\omega}_2(\theta_2+\alpha)} \left(\cos\beta\vec{\omega}_2 + \sin\beta\left(\vec{\omega}_3 \times \vec{\omega}_2\right)\right) = \cos\phi. \tag{7}$$

Let the angle between $\vec{\omega}_1$and $\vec{\omega}_2$ be γ, then (7) becomes (8).

$$\cos\beta\cos\gamma - \frac{\sin\beta}{\sin\gamma}\left[-\cos^2\gamma + \cos(\theta_2+\alpha) + (1-\cos(\theta_2+\alpha))\cos^2\gamma\right] = \cos\phi \tag{8}$$

$$\cos\beta\cos\gamma - \sin\beta\sin\gamma\cos\left(\theta_2+\alpha\right) = \cos\phi. \tag{9}$$

Since $\cos(\theta_2+\alpha) \in [-1,1]$ and $\cos\beta, \cos\gamma, \sin\beta, \sin\gamma > 0$ as $\beta, \gamma \in [0, \frac{\pi}{2}]$, from (9) the range of $\cos\phi$ is

$$\cos\beta\cos\gamma - \sin\beta\sin\gamma \le \cos\phi \le \cos\beta\cos\gamma + \sin\beta\sin\gamma \tag{10}$$

$$\cos\left(\beta+\gamma\right) \le \cos\phi \le \cos\left(\beta-\gamma\right) \tag{12}$$

$$\beta - \gamma \le \phi \le \beta + \gamma. \tag{13}$$

Finally, (12) shows that the range of the polar angle ϕ of the articulating motion depends on β and γ, the angle between $\vec{\omega}_1$ and $\vec{\omega}_2$, and the angle between $\vec{\omega}_2$ and $\vec{P}_0$. In other words, β and γ are the design parameters that determine the range of the articulated motion of the wrist mechanism. The value of β and γ, together with the location of the $\vec{x}_2$ and the interpolation method, determines the shape of the tube.

There are some considerations to determine design parameters, β and γ. First, it is better to have equal β and γ values to have $\phi = 0$, which means that the tool can be pointed in a straight direction. Second, the bigger $\beta + \gamma$ is, the wider range

TABLE I
SPECIFICATION OF PROXIMAL/DISTAL NITINOL TUBE

Tube	Inner diameter (mm)	Outer diameter (mm)	Radius of curvature (mm)	Curvature (mm^{-1})
Distal	0.79	0.94	9.55	0.105
Proximal	1.03	1.24	9.80	0.102
Torque coil	0.55	0.36	-	-

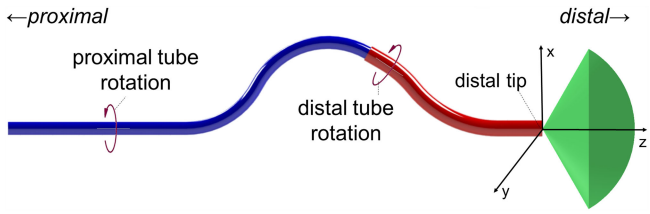

Fig. 3. Shape of the wrist mechanism and its range of articulated motion where $\beta = \gamma = \frac{\pi}{6}$ according to its design parameters of Table I. The range of articulated motion is 120° of pitch angle and the full rotation of the roll angle.

of articulated motion of the mechanism has. Third, a trade-off relationship between the tip's range of articulated motion and manufacturing difficulties should be considered. Increasing the value of β and γ leads to the tube with high curvature, which is difficult to manufacture. Thus, one of the major challenges is to have high curvature of the tubes. Without the high curvature of the tube, the wrist mechanism cannot achieve the desired range of articulated motion.

Considering the required range of articulated motion, we set $\beta = \frac{\pi}{6}$ and $\gamma = \frac{\pi}{6}$ to have the range of the tip's direction for $0 \leq \phi \leq \frac{\pi}{3}$ and $0 \leq \theta \leq 2\pi$. Then, we determine the location of $\vec{x}_2$ at which the proximal tube meets the distal tube considering the manufacturing constraints on the tube curvature. The dimensions of the proximal and distal tubes of the finalized mechanism design are given in Table I, including the curvature of each tube. The diameter of the tube is 1.24 mm, which is smaller than 3–5 mm commercial tools. Fig. 3 demonstrates the shape of the mechanism and the range of articulated motion at the tip according to the determined design parameters. The grey cone demonstrates the proposed wrist's range of articulated motion with the pitch angle range of 120° and full rotations in the roll direction.

C. Forward and Inverse Kinematics of the Wrist Mechanism

Forward kinematics that relates the direction of the tip with the tubes' rotation angle θ_1 and θ_2 is given in (1). To solve the inverse kinematics, the direction of the tool tip is parameterized in spherical coordinate as in (2)

$$\vec{P} = e^{\hat{\omega}_1\theta_1} e^{\hat{\omega}_2\theta_2} \vec{P}_0 = \begin{bmatrix} \sin\phi\cos\theta \\ \sin\phi\sin\theta \\ \cos\phi \end{bmatrix}. \tag{13}$$

We solve the inverse kinematics to calculate the tubes' rotational angle, θ_1 and θ_2, for the given direction of the tip, θ and ϕ In our design, the joint axes are $\vec{\omega}_1 = [0, 0, 1]^T, \vec{\omega}_2 = [-\frac{1}{2}, 0, \frac{\sqrt{3}}{2}]^T$, comparing each component in (13)

$$-\frac{\sin\theta_1\sin\theta_2}{2} + \frac{\sqrt{3}\cos\theta_1\left(\cos\theta_2 - 1\right)}{4} = \sin\phi\cos\theta \tag{14}$$

$$\frac{\cos\theta_1\sin\theta_2}{2} + \frac{\sqrt{3}\sin\theta_1\left(\cos\theta_2 - 1\right)}{4} = \sin\phi\sin\theta \tag{15}$$

$$\frac{\cos\theta_2}{4} + \frac{3}{4} = \cos\phi \tag{16}$$

Solve for θ_2 from (16).

$$\theta_2 = \cos^{-1}\left(4\cos\phi - 3\right). \tag{17}$$

In (17), θ_2 is calculated from the given ϕ value. Given the value of θ, ϕ, θ_2, (14) and (15) can be rearranged as a linear system of (18), which is solved to calculate the value of θ_1

$$\mathbf{A}\left(\theta, \phi, \theta_2\right) \begin{bmatrix} \sin\theta_1 \\ \cos\theta_1 \end{bmatrix} = \boldsymbol{b}\left(\theta, \phi, \theta_2\right). \tag{18}$$

III. MANUFACTURING

As a wrist mechanism for the needlescopic instruments, the mechanism should be able to pass through a straight trocar with inner diameter below 3 mm. Although each link of the wrist mechanism consists of thin tubes, due to the curved shape of the tubes, the volume occupied by the mechanism is larger than the diameter of the tubes comprising the mechanism. As a result, in order for the wrist mechanism to enter the body through a trocar, its links should be straightened during insertion and return to original shape after exiting the trocar. For this reason, the nitinol tube, characterized by superelasticity and biocompatibility, was used to manufacture the proposed mechanism.

A. Asymmetric Laser Patterning for High Curvature

The shape of the links in Table I, resulting from the analysis in the previous section has high curvature. To bend the tubes to the desired high curvature without breaking, the tube's flexural stiffness along the bent direction should be decreased. At the same time, the links should preserve enough torsional stiffness to avoid buckling during rotation. To satisfy such requirements, we applied a partial pattern on the nitinol tubes to create asymmetric flexural stiffness. Two 70°columns per half were patterned like Fig. 4(a). As a result, the flexural stiffness of the tube differs according to its radial direction. Compared to patterning around the entire periphery of the tube, the partial patterning method preserves the torsional flexural stiffness of the tube while enabling the high curvature bending of the tube.

Nd: YVO4 laser source with 355 nm wavelength and linewidth of 20 mm was set up to slit patterns on the nitinol tubes

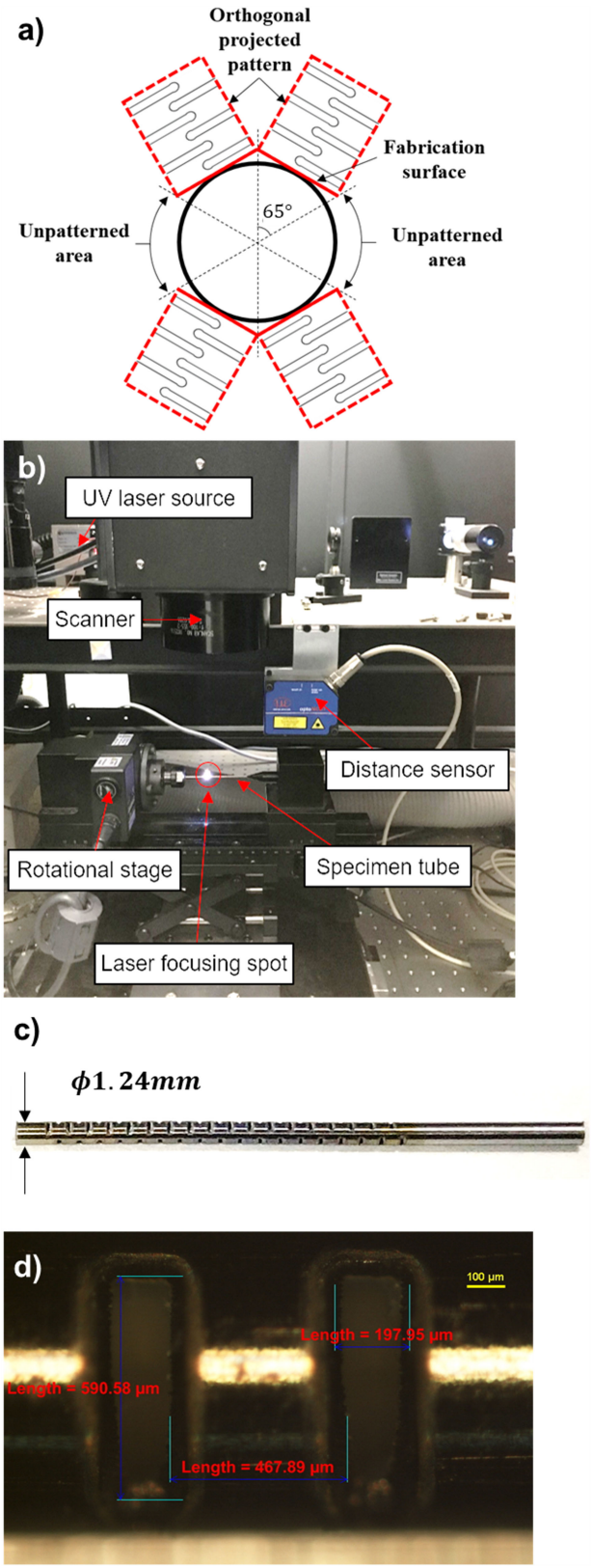

Fig. 4. (a) Asymmetric patterning on the nitinol tubes. Each column of pattern weighs 65°. Two columns are patterned on each half. (b) Laser machining set-ups to engrave patterns on the nitinol tubes. (c) Asymmetrically patterned nitinol tube. (d) Microscopic photograph of the patterned tube.

(AWAVE-355-3W-40K, Advanced Optowave Corporation, NY, USA). The rotational stage rotated a nitinol tube, fixed by collet chuck so that it proceeded laser machining along the surface of the tube. Laser distance sensor set the focus of the laser and the laser scanner shaped the patterns on the nitinol tubes as Fig. 4(b). The patterned tubes were cleansed in an ultrasonic cleaner to get rid of debris. Fig. 4(c) and (d) shows the asymmetrically patterned tube and its microscopic photograph, respectively. The height and length of a single pattern are approximately 198 and 591 μm, respectively.

The pattern design determines the flexural stiffness of the tube and subsequently the maximum curvature of tubes. The relationship between the shape of the patterns and the stiffness of the tube is studied in our previous works [26], [27]. Thus, depending on the required shape of the mechanism, the pattern design can be customized.

B. Heat Treatment to Shape High Curvature of the Tubes

To set the shape of the tube to designed high curvature, the patterned tube was placed in a jig, annealed in the furnace for 28 minutes at 530 °C, and then quenched in room temperature water. Since the high curvature cannot be shaped by a single heat treatment process, we went through the heat treatment process twice: the first used a low curvature jig and the second used a high curvature jig. After the two heat treatment steps, both the proximal and distal tubes were shaped into the designated design. Fig. 5(a) and (b) shows the proximal and distal tubes from the second heat treatment with the high curvature jigs. The tubes have no fracture or failure because the patterns reduce the flexural stiffness of the tubes along the bending direction.

C. Assembly of the Wrist Mechanism

The proximal and distal tubes are assembled coaxially as we designed in Fig. 5(c). Each curved tube was connected with a separate straight stainless steel tube controlled by a motor. The distal curved tube was connected with three-layered torque coil (Asahi Intecc, Japan) so that torque from the proximal end transmits to the distal tube located at the distal end. The torque coil was fixed to a straight stainless steel tube which is held by a collet chuck attached to the motor. Then, the torque coil went through the curved proximal tube and was connected to the distal tube. The assembled mechanism is presented in Figs. 5(c) and 7(a). The forceps with actuating wire are equipped as an end-effector. The actuating wires of the forceps pass from proximal end to distal end through the hollow structure of the torque coil.

Due to the superelasticity of the nitinol, even though the two tubes are very high curved structure, they can be straightened during invading into the body with a straight guide tube as shown in Fig. 6. When it reaches the target, the tube returns to its original high-curved shape. The asymmetric patterning allows the mechanism to switch between straighten form and high curved form according to situations. The method reduces the diameter of the mechanism to minimize invasiveness during the surgical process.

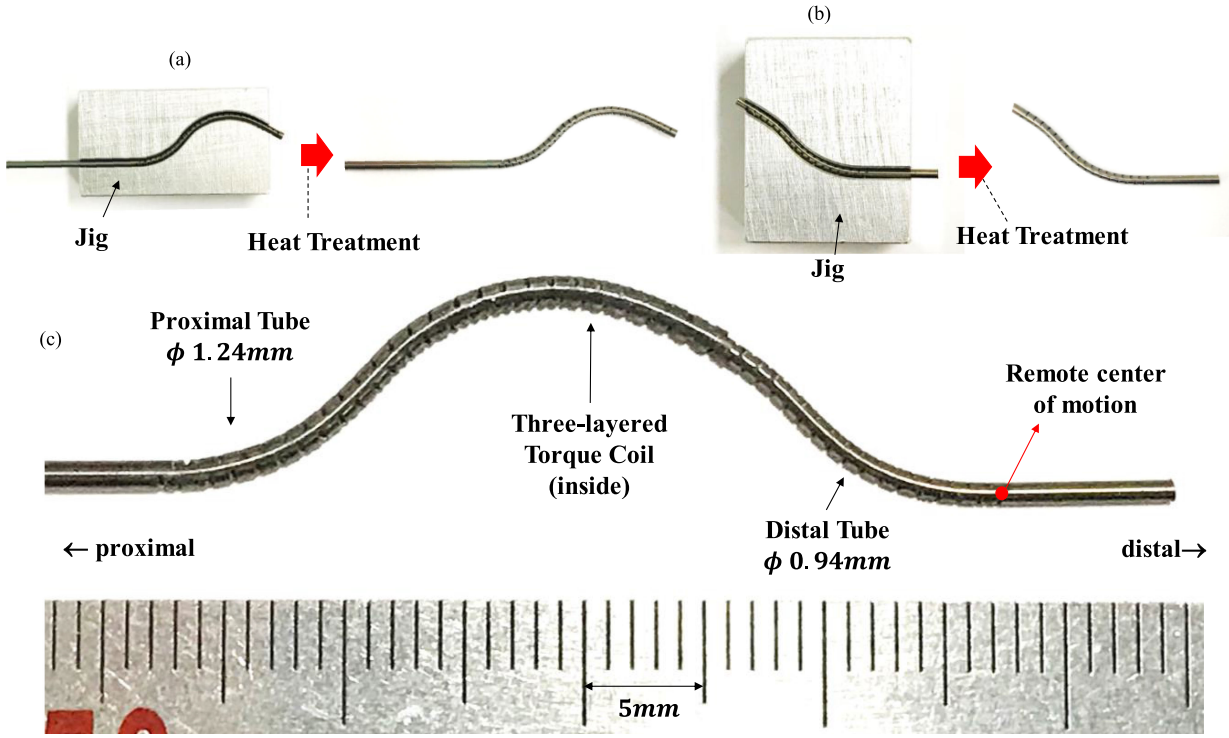

Fig. 5. (a) Second heat treatment jig to shape the proximal tube (ϕ1.24 mm) with the radius of curvature of 9.80 mm. (b) Second heat treatment jig to shape the proximal tube (ϕ 0.94 mm) with the radius of curvature of 9.55 mm. (c) It represents the assembled wrist mechanism. The torque coil passes through the proximal tube and gets connected to the distal tube to transmit torque from the proximal.

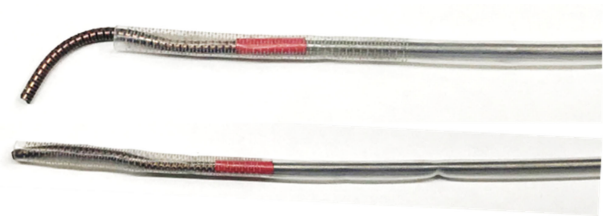

Fig. 6. Using a guide tube, the high curved nitinol tube (upper) is straightened during invasion (lower) to minimize invasiveness.

TABLE II
MANUFACTURING PROCESS OF THE WRIST MECHANISM

1)	Asymmetric patterning on nitionl tubes by UV laser machining
2)	1st annealing: Heat treating the patterned tube with low curvature at 530 °C for 28 minutes in furnace and then quenching in the water
3)	2nd annealing: Heat treating the tube with high curvature jig at 530 °C for 28 minutes in furnace and then quenching in the water
4)	The distal tube is connected with torque coil and assembled with the proximal tube coaxially.
5)	An end effector (grippers) is equipped at the distal end. The activating wire passes through hollow space of the torque coil.
6)	Integrate the mechanism with the motor-controller. Each tube is controlled by a separate motor. The gripper is controlled by an additional motor.
7)	Build the teleoperated control system using 6-axis robot arms and haptic devices.

The assembled mechanism was integrated with the controller with three motors for control. Finally, the system was integrated with the six-axis robot arm, Denso robotics versus series (Denso Robotics, CA, USA), and Sensable Phantom Omni haptic device (3-D Systems, SC, USA) to build the master/slave control system. The system enables the teleoperated control of the wrist. In summary, Table II sums up the manufacturing process of the 2R wrist mechanism.

IV. CONTROL OF THE WRIST MECHANISM

A. Control System for the Wrist Mechanism

The wrist mechanism was controlled by two rotational motors and the grippers were actuated by an additional motor. The separate motor held each tube by a collet chuck and controlled the rotation of the tube independently. The motors were graphite brushes Maxon Motor of 4.5 W and ϕ 16 mm (part number:118730) with the 512 counts-per-turn encoder (part number: 201937). The gear head with 19:1 reduction ratio was used. Alternatively, we also used the motors of Dynamixel MX-28AR. The encoder of each motor indicated the rotation angle of each tube. Controller board communicating with Linux PC through RS-485 communication controls the motors. An additional motor controlled the translational movement of the activating wire

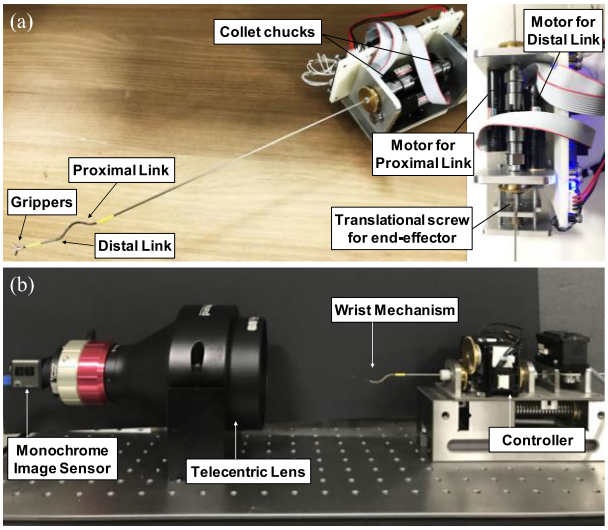

Fig. 7. (a) Wrist mechanism with the grippers were integrated to the motor controller. Two motors controlled the rotation of the two links. The additional motor actuated the grippers. (b) Telecentric lens with monochrome image sensor was installed to measure the direction of the tip at *x*–*z* and *x*–*y* planes.

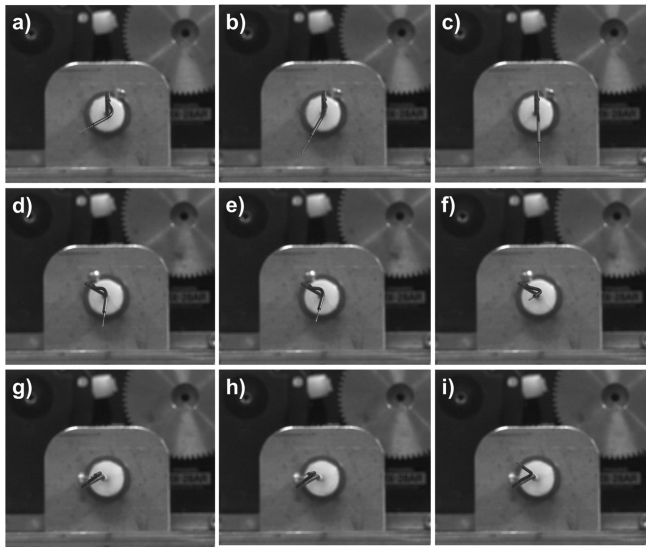

Fig. 8. Telecentric lens images of the direction of the distal tip for the given rotated angles of the two links, $(\theta_1,\ \theta_2)$. (a) $(\theta_1,\theta_2)= (0, 60)$, (b) $(0, 120)$, (c) $(0, 180)$, (d) $(60, 60)$,e) $(60, 120)$, (f) $(60, 180)$, (g) $(120, 60)$, (h) $(120, 120)$, and (i) $(120\ ,\ 180\ )$.

to fold and unfold the grippers. Fig. 7(a) demonstrates that the mechanism was equipped with the controller.

For teleoperation, relative translation of the stylus is mapped to the translation of the wrist mechanism by the robot arm. The stylus of the haptic device has three-DoFs rotation, and the relative rotation of the stylus by its first three-DoFs is mapped to the increment of the orientation of the wrist. The operator can also fold/unfold the graspers by pressing the button of the stylus to pull/loosen the wire. The feasibility of the teleoperated system was verified by the peg transfer test shown in Fig. 9 and in complementary multimedia.

B. Validation of the Kinematics

We performed experiments to verify our kinematics model. The wrist was moved to specific joint coordinates. Then, the direction of the distal tip was experimentally measured and compared to the direction computed by kinematics. The camera was set to record the distal tip's projected direction in the *x*–*y* plane and the *x*–*z* plane of frame {b} defined in Fig. 2(c). Specifically, the telecentric lens (0.09X ½" GoldTL Telecentric Lens, Edmund Optics, NJ, USA) with a monochrome image sensor (EO-1312M, Edmund Optics, NJ, USA) was installed to take an image of the tip at *x*–*z* and *x*–*y* planes as Fig. 7(b). The monochrome image sensor is suitable for high resolution of the enlarged image. From the images, we measured the tip's direction about *z*-axis and *x*-axis. We measured θ and ϕ from the pictures taken in the *x*–*y* and *x*–*z* planes, respectively. In the *x*–*y* plane, the angle between the projected direction and *x*-axis is θ. In the *x*–*z* plane, let the angle between the projected direction and *z*-axis be α. Then, ϕ is determined as

$$\phi = \tan^{-1}\left(\tan\alpha/\cos\theta\right). \tag{19}$$

TABLE III
COMPARISON OF THE DIRECTION OF THE DISTAL TIP BETWEEN THEORETICAL AND EXPERIMENTAL RESULTS

#	Rotated angle (°)		Theoretical Tip Direction (°)	Experimental Tip Direction (°)	Angle differ-ence (°)
	θ_1	θ_2	(ϕ, θ)	(ϕ, θ); *std*	-
1	0	60	(29.0, 116.6)	(32.5, 119.0); 2.24	4.06
2	0	120	(51.3, 146.3)	(53.2, 149.1); 1.85	2.56
3	0	180	(60.0, 180.0)	(61.8,181.8); 2.60	2.00
4	60	60	(29.0, 176.6)	(32.2, 172.7); 1.93	4.64
5	60	120	(51.3, 153.7)	(54.5, 162.8); 2.91	6.34
6	60	180	(60.0, 120.0)	(57.4,123.1); 2.29	3.06
7	120	60	(29.0, 123.4)	(27.0, 116.7); 3.25	6.24
8	120	120	(51.3, 93.7)	(54.1,100.3); 2.89	4.88
9	120	180	(60.0, 60.0)	(57.2, 55.7); 2.18	3.58

For a given set of the rotation angles θ_1 and θ_2, where $\theta_1 \in \{0°, 60°, 120°\}$ and $\theta_2 \in \{60°, 120°, 180°\}$, we calculated the direction of the tip using its kinematics (13)–(18), and, simultaneously, measured the direction of the tip using (19). Fig. 8 shows the photographs from the telecentric lens to represent the direction of the tip at the RCM for the given cases. Table III compares the theoretical and experimental tip direction in spherical coordinate, and the difference angle between the two direction vectors. For each case, the experimental tip direction was measured by five times and the average and the standard deviation of the experimental tip direction vector is given in Table III. The result showed the consistency between the experimental and theoretical results. The average angle difference between experimental and theoretical value was 4.15° and its standard deviation was 1.53°. Additionally, the supplementary

video demonstrates the full workspace of the wrist with the random sinusoidal functions for the rotated angles of the tubes.

The location of the RCM point, which is the pivot point of the tip motion, should ideally remain stationary during the experiments. Although it was difficult to measure the three-dimensional position of the RCM point during the experiments, in the x–z plane photographs, we observed that the RCM did not deviate more than 2 mm from the center.

There are two main factors that contribute to the difference between the experiments and the theoretical tip direction and RCM point locations. The first is the geometrical errors that originate from the gap between the tubes and the deviation of the tube curvature from the original design. Such errors can be reduced by improved manufacturing methods, such as Femto UV laser machining and advanced heat treatment. The second is the loss of the rotational motion of the distal link actuated by the torque coil. While the torque coils are very good for transmitting rotation through the curved path, high curvature of the proximal tube that it passes through and the friction between the coil and the inner walls of the proximal tube inevitably creates the discrepancy between the commanded and actual rotation of the distal tube. Optimal design of the torque coil and lubrication need to be studied to reduce this error.

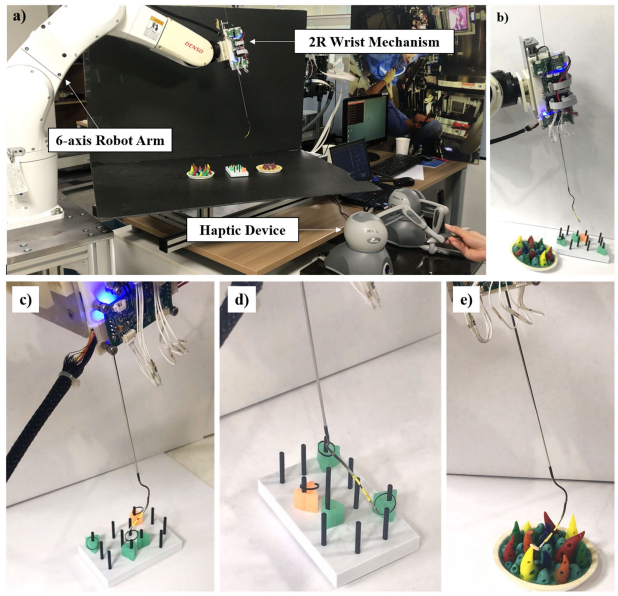

Fig. 9. (a) and (b) Wrist mechanism was integrated with the robot arm and the haptic device to build the master/slave teleoperated control system. (c), (d), and (e) Peg transfer test was performed by the built robotic system in various environments.

C. Peg Transfer Test With the Teleoperated Control System

To test the feasibility of the wrist as the microsurgical instruments, we performed the peg transfer study with the robotic trainer box (The Chamberlain Group, Inc., MA, USA). Using the built teleoperated control system, an operator manipulated the stylus to control the 1.24-mm diameter wrist mechanism with the grippers. The goal of the test was to demonstrate the feasibility of the mechanism for microlaparoscopy. The supplementary video and Fig. 9 show the teleoperated surgical robot equipped with the presented wrist transferring small rings from one peg to another. The small and delicate sensors [28]–[30] are expected to improve the control system through force feedback.

V. Discussion

In this article, we present a two-DoF wrist mechanism (ϕ1.24 mm) consisting of highly curved links serially connected by rotary joints. The two main characteristics of the presented mechanism are the kinematic tractability and the sharp articulating motion about the RCM. At first, the serial robot structure of the mechanism provides an analytic solution for forward and inverse kinematics, making it easier to control. Second, the links of the mechanism are designed to create an RCM near the position of the end-effector. While satisfying the trocar orientation requirement, the wrist undergoes large reorientations with minimal displacement of the end-effector that is close to a pivot point.

The fabricated wrist has the articulated motion with the pitch angle range of 120° and full rotations in the roll direction. Furthermore, using the superelasticity of the nitinol tubes, the proposed mechanism can be straightened to fit into 2 mm-trocar for minimally invasive introduction into the body. The kinematics of the mechanism was verified by the experiments. The measure tip directions were consistent with that calculated by kinematics. Finally, the feasibility of the mechanism for microlaparoscopy was demonstrated by the peg transfer test using the teleoperated robotic control system equipped with the proposed wrist.

One limitation of the presented mechanism is large motion envelope during its operation due to its curved links. Still, the mechanism can be straightened to fit into a trocar for deployment. The application of the mechanism is appropriate for the surgeries where the operating space of the tool is wide once the tool passes through the long and narrow passage. In particular, laparoscopic surgery has a large abdominal cavity that allows wider range of motion of the mechanism after the mechanism has been straightened to pass through a very small trocar. Thus, microlaparoscopic surgery is an exemplary surgery with this 1.24-mm diameter wrist and the feasibility was tested in peg transfer experiment in Section IV-C.

In future work, we plan to study the optimal geometry of the tubes compromising the mechanisms in terms of motion envelope. In the article, the bending of both the proximal and distal tubes was limited to planar bending. On the other hand, spatially curved tubular links are expected to minimize the motion envelope of the wrist mechanism. If the shape of the tube is three-dimensionally curved, one can optimize the motion envelope and customize the design of the wrist mechanism according to target applications.

Finally, in conjunction with a medical team, we plan to perform phantom tests, including a cadaver test. With surgeons, we will verify the usability and functionality of the proposed wrist mechanism to appreciate the impact in patient care. Utilizing the wrist mechanism, it aims to expand the scope of robotic surgery, especially in microlaparoscopic surgery.

ACKNOWLEDGMENT

The Institute of Engineering Research at Seoul National University provided research facilities for this work.

REFERENCES

[1] E. Kanehira, T. Tanida, A. Kamei, M. Nakagi, T. Yoshida, and S. Touma, "Needlescopic intragastric surgery facilitated by newly developed 2 mm instruments," *Minimally Invasive Therapy. Allied Technol.*, vol. 25, no. 4, pp. 210–214, Jul. 2016.

[2] N. Tagaya and K. Kubota, "Reevaluation of needlescopic surgery," *Surg. Endoscopy*, vol. 26, no. 1, pp. 137–143, Jan. 2012.

[3] Y.-W. Chan and C. Hollinsky, "Needlescopic surgery versus single-port laparoscopy for inguinal hernia," *J. Soc. Laparoendscopic Surgeons*, vol. 19, no. 3, Sep. 2015, Art. no. e2015.00056.

[4] A. Üneri, M. A. Balicki, J. Handa, P. Gehlbach, R. H. Taylor, and I. Iordachita, "New steady-hand eye robot with micro-force sensing for vitreoretinal surgery," in *Proc. 3rd IEEE RAS EMBS Int. Conf. Biomed. Robot. Biomechatronics*, 2010, pp. 814–819.

[5] P. Valdastri, R. J. W. III, C. Quaglia, M. Quirini, A. Menciassi, and P. Dario, "A new mechanism for mesoscale legged locomotion in compliant tubular environments," *IEEE Trans. Robot.*, vol. 25, no. 5, pp. 1047–1057, Oct. 2009.

[6] S. Asai, H. Ishimoto, A. Yabuno, H. Asada, M. Mikami, and Y. Yoshimura, "A novel modification of two-port laparoscopic ovarian cystectomy using a needlescopic instrument: One surgeon's initial experience," *Gynecol. Minimally Invasive Therapy*, vol. 5, no. 3, pp. 120–123, Aug. 2016.

[7] M. Piccigallo *et al.*, "Design of a novel bimanual robotic system for single-port laparoscopy," *IEEE ASME Trans. Mechatron.*, vol. 15, no. 6, pp. 871–878, Dec. 2010.

[8] J. Kim, Y. Nakajima, and K. Kobayashi, "A suction-fixing, stiffness-tunable liver manipulator for laparoscopic surgeries," *IEEE ASME Trans. Mechatron.*, vol. 23, no. 1, pp. 262–273, Feb. 2018.

[9] K. Xu, J. Zhao, and M. Fu, "Development of the SJTU unfoldable robotic system (SURS) for single port laparoscopy," *IEEE ASME Trans. Mechatron.*, vol. 20, no. 5, pp. 2133–2145, Oct. 2015.

[10] M. Khoshnam and R. V. Patel, "Robotics-assisted control of steerable ablation catheters based on the analysis of tendon-sheath transmission mechanisms," *IEEE ASME Trans. Mechatron.*, vol. 22, no. 3, pp. 1473–1484, Jun. 2017.

[11] B. L. Conrad and M. R. Zinn, "Interleaved continuum-rigid manipulation: an approach to increase the capability of minimally invasive surgical systems," *IEEE ASME Trans. Mechatron.*, vol. 22, no. 1, pp. 29–40, Feb. 2017.

[12] J. Burgner *et al.*, "A telerobotic system for transnasal surgery," *IEEE ASME Trans. Mechatron.*, vol. 19, no. 3, pp. 996–1006, Jun. 2014.

[13] "Intuitive Surgical - Endowrist Instruments," [Online]. Available: https://www.intuitivesurgical.com/products/instruments/. Accessed: Apr. 6, 2018.

[14] "Tuebingen Scientific: Radius T," [Online]. Available: http://www.tuebingen-scientific.com/index.php?id = 68. Accessed: Apr. 26, 2018.

[15] "FlexDex Surgical – The MIS Device that Moves Like You," [Online]. Available: https://flexdex.com/. Accessed: 26, 2018.

[16] "SILSTM Hand Instruments | Medtronic," [Online]. Available: http://www.medtronic.com/covidien/en-us/products/hand-instruments-ligation/sils-hand-instruments.html. Accessed: Apr. 26, 2018.

[17] P. J. Swaney, P. A. York, H. B. Gilbert, J. Burgner-Kahrs, and R. J. Webster, "Design, fabrication, and testing of a needle-sized wrist for surgical instruments," *J. Med. Devices*, vol. 11, no. 1, Dec. 2016, Art. no. 014501.

[18] "MMI Microinstruments," MMI Microinstruments. [Online]. Available: http://www.mmimicro.com/. Accessed: May 7, 2018.

[19] "Percutaneous intracardiac beating-heart surgery using metal MEMS tissue approximation tools - Andrew H Gosline, Nikolay V Vasilyev, Evan J Butler, Chris Folk, Adam Cohen, Rich Chen, Nora Lang, Pedro J del Nido, Pierre E Dupont, 2012. [Online]. Available: http://journals.sagepub.com/doi/abs/10.1177/0278364912443718. Accessed: Apr. 12, 2018.

[20] J. Burgner-Kahrs, D. C. Rucker, and H. Choset, "Continuum robots for medical applications: A survey," *IEEE Trans. Robot.*, vol. 31, no. 6, pp. 1261–1280, Dec. 2015.

[21] P. A. York, P. J. Swaney, H. B. Gilbert, and R. J. Webster, "A wrist for needle-sized surgical robots," in *Proc. IEEE Int. Conf. Robot. Autom. ICRA Proc. IEEE Int. Conf. Robot. Autom.*, May 2015, vol. 2015, pp. 1776–1781.

[22] P. E. Dupont, J. Lock, B. Itkowitz, and E. Butler, "Design and control of concentric-tube robots," *IEEE Trans. Robot.*, vol. 26, no. 2, pp. 209–225, Apr. 2010.

[23] R. J. W. III, J. M. Romano, and N. J. Cowan, "Mechanics of precurved-tube continuum robots," *IEEE Trans. Robot.*, vol. 25, no. 1, pp. 67–78, Feb. 2009.

[24] "Torque Coil." [Online]. Available: http://www.asahi-inteccusa.com/index.php?option = com_content&view = article&id = 71&Itemid = 67. Accessed: Mar. 11 2019.

[25] R. M. Murray, *A Mathematical Introduction to Robotic Manipulation*, 1st ed. Boca Raton, FL, USA: CRC Press, 1994.

[26] J.-S. Kim, D.-Y. Lee, K. Kim, S. Kang, and K.-J. Cho, "Toward a solution to the snapping problem in a concentric-tube continuum robot: Grooved tubes with anisotropy," in *Proc. 2014 IEEE Int. Conf. Robot. Automat.*, 2014, pp. 5871–5876.

[27] D.-Y. Lee *et al.*, "Anisotropic patterning to reduce instability of concentric-tube robots," *IEEE Trans. Robot.*, vol. 31, no. 6, pp. 1311–1323, Dec. 2015.

[28] U. Kim, D. H. Lee, Y. B. Kim, D. Y. Seok, and H. R. Choi, "A novel six-axis force/torque sensor for robotic applications," *IEEE ASME Trans. Mechatron.*, vol. 22, no. 3, pp. 1381–1391, Jun. 2017.

[29] N. Kumar, O. Piccin, L. Meylheuc, L. Barbé, and B. Bayle, "Design and modeling of a polymer force sensor," *IEEE ASME Trans. Mechatron.*, vol. 21, no. 1, pp. 555–564, Feb. 2016.

[30] A. S. Naidu, R. V. Patel, and M. D. Naish, "Low-cost disposable tactile sensors for palpation in minimally invasive surgery," *IEEE ASME Trans. Mechatron.*, vol. 22, no. 1, pp. 127–137, Feb. 2017.

Jongwoo Kim (S'14–M'19) received the B.S., M.S., and Ph.D. degrees in mechanical and aerospace engineering from Seoul National University, Seoul, South Korea, in 2013, and 2019, respectively.

He is currently a Postdoctoral Research Fellow with the Center for Image-Guided Innovation and Therapeutic Intervention, the Hospital for Sick Children, Toronto, ON, Canada. His current research interests include surgical robotics, medical devices, soft robotics, and novel mechanisms using smart structures.

Dr. Kim was the recipient of the Global Ph.D. Fellowship from National Research Foundation of Korea.

Woosub Lee received the B.S. degree in mechanical engineering from Sogang University, Seoul, South Korea, in 1999, the M.S. degree in electronic engineering from Yonsei University, Seoul, South Korea, in 2004, and the Ph.D. degree in mechanical and aerospace engineering from the Tokyo Institute of Technology, Tokyo, Japan, in 2013.

Since 2004, he has been with the Korea Institute of Science and Technology, Seoul, South Korea, where he is currently a Senior Research Scientist. His current research interests include creative robot mechanism design, reliable motion control systems, and field robot systems for hazardous duty.

Sungchul Kang (M'06) received the B.S., M.S. and Ph.D. degrees in mechanical design and production engineering from Seoul National University, Korea, in 1989, 1991, and 1998, respectively.

From 1991 to March 2019, he conducted robotics research at the Korea Institute of Science and Technology. Since April 2019, he has been with the Robot Center, Samsung Research. His research interests include manipulation for medical and service robots based on mechanism design and control.

Kyu-Jin Cho (M'08) received the B.S. and M.S. degrees from Seoul National University, Seoul, South Korea, in 1998 and 2000, respectively, and the Ph.D. degree from the Massachusetts Institute of Technology, Cambridge, MA, USA, in 2007, all in mechanical engineering.

He was a Postdoctoral Fellow with the Harvard Microrobotics Laboratory until 2008. He is currently a Professor of mechanical and aerospace engineering and the Director of the BioRobotics Laboratory and Soft Robotics Research Center, Seoul National University. His research interests include biologically inspired robotics, soft robotics, soft wearable devices, novel mechanisms using smart structures, and rehabilitation and assistive robotics.

Dr. Cho was the recipient of the 2014 IEEE RAS Early Academic Career Award, 2014 ASME Compliant Mechanism Award, 2013 IROS Best Video Award, and 2013 KSPE Paik Am Award.

Chunwoo Kim (M'18) received the B.S. degree in mechanical aerospace engineering from Seoul National University, Seoul, South Korea, in 2008, and the Ph.D. degree in mechanical engineering from Johns Hopkins University, Baltimore, MD, USA, in 2014.

He is currently with the Center for Medical Robotics, Korea Institute of Science and Technology, Seoul, South Korea. His research interests include image-guided robots, surgical robots, and medical devices.

Dr. Kim was the recipient of a Fulbright Scholarship and the Prostate Cancer Research Training Award of the United States Department of Defense.